PROCEEDINGS OF SCIENCE

Physics overview of J-PARC

Kazuya Aoki*

High Energy Accelerator Research Organization (KEK),
1-1 Oho, Tsukuba, Ibaraki, 305-0801, Japan

E-mail: kazuya.aoki@kek.jp

J-PARC, Japan Proton Accelerator Research Organization, is located at Tokai village, Ibaraki, Japan, co-hosted by JAEA and KEK. J-PARC can provide proton beams with a kinetic energy of up to 30 GeV, as well as various secondary beams. J-PARC Hadron experimental facility hosts nuclear and particle physics experiments to understand strongly interacting particle systems from quarks to neutron stars. This manuscript discusses some of the recent results from the J-PARC Hadron experimental facility, along with ongoing and future projects.

The XVIth Quark Confinement and the Hadron Spectrum Conference (QCHSC24)
19-24 August, 2024
Cairns Convention Centre, Cairns, Queensland, Australia

*Speaker

 ISSN 1824-8039 . Published by SISSA Medialab.

PoS(QCHSC24)017

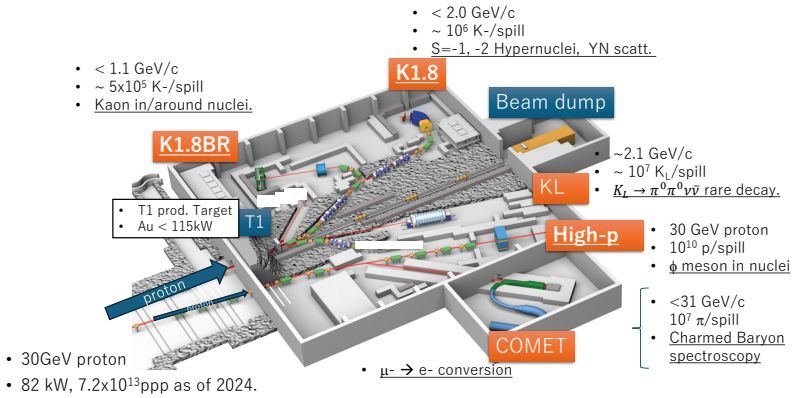

Figure 1: Hadron experimental facility and its beamlines. 30 GeV proton from MR bombards the production target T1 and provides secondary beams to K1.8, K1.8BR, KL beamlines. Primary proton beamline provides 30 GeV proton beams to high-p beamline, and 8 GeV to COMET beamline.

1. Introduction

1.1 J-PARC

J-PARC, Japan Proton Accelerator Research Organization, is located at Tokai village, Ibaraki, Japan, co-hosted by JAEA and KEK. The proton beam gradually accelerates through 400-MeV Linac, 3-GeV Rapid Cycle Synchrotron (RCS), and 30-GeV Main Ring (MR).

J-PARC has three major experimental facilities: MLF for the Material and Life science experimental Facility, NU for the Neutrino experimental facility, and HD for the Hadron experimental facility. MLF accepts beams from RCS, NU and HD accepts beams from MR. Although MLF mainly focuses on materials and life sciences, it hosts nuclear and particle experiments such as $g-2$ [1], a sterile neutrino search JSNS^2 [2], and a direct measurement of neutron life [3]. NU provides ν or $\bar{\nu}$ beam and shoots them at Super Kamiokande located 295 km away from J-PARC to measure neutrino oscillation. HD hosts nuclear and particle experiments. The approval summary of experiments at HD and NU can be found in [4]. This manuscript reviews some of the recent results at HD and discusses them along with current and future physics programs.

1.2 HD - hadron experimental facility

Figure 1 illustrates the hadron experimental facility and its beamlines. The proton beam of MR is slowly extracted and directed to HD. As of 2024, the beam power was 82 kW, 7.2×10^{13} protons for a two-second spill. The primary proton beam bombers a production target of HD, T1, creating various secondary particles such as pions and kaons. These secondary particles are provided to K1.8 (Sec. 3), K1.8BR (Sec. 4) and KL beam lines. K1.8 beam line can deliver mass-separated particles up to 2.0 GeV/c. Its double electric separator provides high-purity kaons with K/π ratio at the order of 1 at an intensity of up to 10^6/spill. $S=-1$ and $S=-2$ hypernuclear spectroscopy and hyperon scattering experiments are conducted. K1.8BR delivers mass-separated particles up to 1.1 GeV/c. Its short beam line is advantageous for providing intense low-energy particles. Kaonic nuclei and kaonic atom experiments are conducted in K1.8BR. KL beamline provides K_L and the

KOTO experiment is conducted to search for new physics beyond the standard model (BSM) by observing a CP violating rare decay, $K_L \to \pi^0 \nu\bar{\nu}$ [5]. A small portion of primary proton beams are separated using a Lambertson magnet [6] and extracted to the high-p beam line (Sec. 5). In-medium spectral change of vector mesons is studied. The beamline will be upgraded to provide high-energy secondary beams of up to 31 GeV/c, and charmed baryon spectroscopy is planned [7].

Section 2 discusses the physics motivation of the J-PARC HD experiments. Section 3 reviews experiments conducted at the K1.8 beamline, after providing an overview of their methodology. Section 4 describes experiments conducted at K1.8BR. Section 5 explains an ongoing experiment at high-p. Section 6 introduces future plans of HD.

2. Physics Motivation

The objective of the experiments conducted at HD is to understand strongly interacting systems from quarks to neutron stars. It naturally involves multiple energy scales, and appropriate degrees of freedom have to be chosen to understand the corresponding scales. Various experiments were conducted and planned to deepen our understanding of the system.

Quarks and gluons form hadrons. Quantum Chromodynamics (QCD) is the fundamental theory of such a system, yet its non-perturbative and many-body nature makes the system elusive. The non-trivial QCD vacuum structure, where chiral symmetry is spontaneously broken, plays a crucial role. J-PARC E16 (Sec. 5.1) will give insights using mesons in the medium as a probe. Constituent quarks emerge in hadrons, and the interactions are studied by spectroscopy [7]. At the hadron level, baryon-baryon (BB) and meson-baryon (MB) interactions have to be studied. It was confirmed only recently that exotic hadrons exist, whose constituent quark structure differs from qqq or $\bar{q}q$. At the same time, $\Lambda(1405)$ is now considered as a meson-baryon $\bar{K}N$ molecular state rather than a multi-quark state. J-PARC E15 (Sec. 4.1) confirmed the existence of a larger kaonic nucleus, $\bar{K}NN$. A neutron star (NS) has a highly dense core whose density is several times the nuclear saturation density. Hyperons would emerge, but they makes the system too soft to support heavy NS based on the current knowledge, known as the hyperon puzzle. Detailed hadron interaction study, including Y, is crucial in obtaining a microscopic understanding of such extreme conditions. YN interaction is intensively studied by hypernuclear spectroscopy. J-PARC E13 (Sec. 3.3) confirmed a large charge symmetry breaking in ΛN interactions in ${}^{4}_{\Lambda}\mathrm{H}$ and ${}^{4}_{\Lambda}\mathrm{He}$. J-PARC E05 (Sec. 3.5) measured Ξ^- hypernucleus by nuclear emulsion. The effort continues to use counters in J-PARC E07 and J-PARC E70 (Sec. 3.4). J-PARC E40 (Sec. 3.2) conducted YN scattering experiment to directly study YN interactions. These J-PARC efforts, together with theoretical and worldwide experimental studies, are made for the understanding of the strongly interacting matter at multiple energy scales.

3. K1.8 beamline: strangeness nuclear physics

3.1 Overview

The main focus of experiments at K1.8 is the strangeness nuclear physics. Hypernuclear spectroscopy and hyperon-nucleon (YN) scattering experiments are performed to study BB interactions, extending the traditional NN world by including hyperons. The following three types of reactions are typically used to create hyperons and hypernucleus.

(K^-, π) **reaction; creation of** $S = -1$ **system**: The s quark is already in the beam particle, and it stays in the system of interest, creating a $S = -1$ system. Momentum transfer is small.

(π, K^+) **reaction; creation of** $S = -1$ **system**: The $s\bar{s}$ pair is created in the reaction, and the out-going K^+ takes away $\bar{s}$. The s quark remains in the system of interest, creating $S = -1$ system. Momentum transfer is large, and excited states are more populated compared to (K^-, π).

(K^-, K^+) **reaction; creation of** $S = -2$ **system**: The s quark is in the beam, and $s\bar{s}$ are pair created. K^+ takes away the $\bar{s}$ quark. Therefore, two s quarks remain in the system of interest.

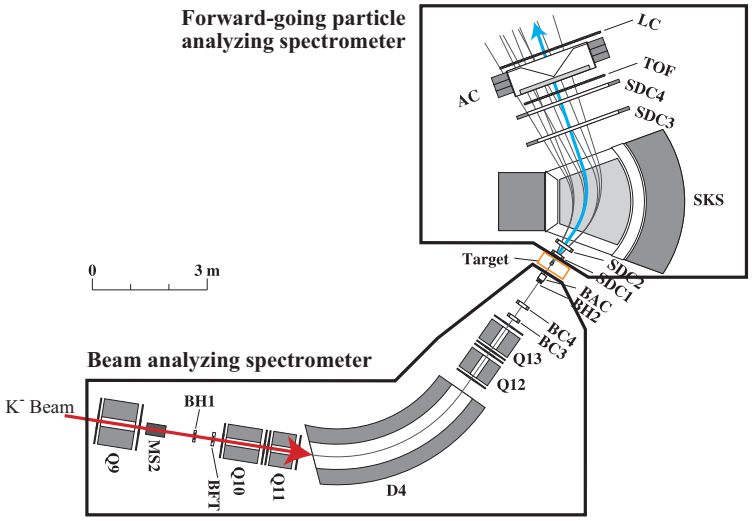

Figure 2: Typical experimental setup at K1.8. It consists of a beam-analyzing spectrometer, an experimental target, and a forward-going particle analyzing spectrometer. When experiment-specific measurements are necessary, additional detectors are placed around the experimental target. Modified based on [25] (CC4.0).

Figure 2 shows a typical experimental setup of K1.8 experiments. The incoming beam is analyzed by a beamline spectrometer, which consists of bending and focusing magnets and position-sensitive and particle identification detectors. Downstream of a target, an experiment-specific spectrometer is prepared to analyze outgoing particles, making missing mass measurement possible. Additional experiment-specific detectors may surround the target. J-PARC E13 placed Hyperball-J (Sec.3.3). The J-PARC E40 experiment installed CATCH detectors (Sec. 3.2) around their targets.

3.2 J-PARC E40 experiment - $\Sigma^\pm p$ elastic and inelastic scatterings

J-PARC E40 experiment measured differential cross-sections of $\Sigma^\pm p$ elastic scatterings and $\Sigma^- p \to \Lambda n$ inelastic scattering. These data are important in constraining yet undetermined low energy constants (LECs) in chiral effective field theory (EFT). Octet baryon pair can be categorized in $\mathrm{SU}_f(3)$ into $\mathbf{8} \otimes \mathbf{8} = \mathbf{27} \oplus \mathbf{10}^* \oplus \mathbf{10} \oplus \mathbf{8_s} \oplus \mathbf{8_a} \oplus \mathbf{1}$. Table 1 summarizes contributing components. In NN intearctions only 27- and 10^*-plets contributes. Bound states of Σ hypernucleus are very rare, making scattering experiments an important source of information.

The $\Sigma^\pm$ beams are produced at liquid hydrogen target as $\pi^\pm p \to K^+ \Sigma^\pm$. The beamline spectrometer analyzes $\pi^\pm$, and the downstream spectrometer, KURAMA, analyzed the out-going K^+, enabling missing mass calculation to identify $\Sigma^\pm$. Σp scatterings were tagged by a detector system called CATCH [8], which surrounds the target. It comprises an innermost cylindrical fiber

tracker (CFT), BGO calorimeters, and pi-identification hodoscopes (PiID). 4500 events of $\Sigma^- p \to \Sigma^- p$ reactions [9], 2400 events of $\Sigma^+ p \to \Sigma^+ p$ [10], and 1000 events of $\Sigma^- p \to \Lambda n$ reactions [11] were accumulated. Figure 3 shows differential cross sections for $\Sigma^- p$ elastic scatterings. Compared to previous measurements, E40 data significantly improves angular coverage and statistical accuracy.

Table 1: Contributions to baryon-baryon interactions from $SU_f(3)$ multiplets.

B-B (I)	spin/OAM = 0/even or 1/odd	spin/OAM = 1/even or 0/odd
NN ($I=0$)	–	$[\mathbf{10}^*]$
NN ($I=1$)	$[\mathbf{27}]$	–
ΛN ($I=1/2$)	$\frac{1}{\sqrt{10}}([\mathbf{8_s}]+3[\mathbf{27}])$	$\frac{1}{2}(-[\mathbf{8_a}]+[\mathbf{10}^*])$
ΣN ($I=1/2$)	$\frac{1}{\sqrt{10}}(3[\mathbf{8_s}]-[\mathbf{27}])$	$\frac{1}{2}([\mathbf{8_a}]+[\mathbf{10}^*])$
ΣN ($I=3/2$)	$[\mathbf{27}]$	$[\mathbf{10}]$

Such systematic and precise data stimulated theoretical efforts to go beyond NLO in chiral EFT. Figure 4 shows NLO and NNLO EFT calculations [12], compared with the E40 data. Solid red lines are NNLO obtained with fit to E40 data, showing good agreement. Cyan bands are NLO19 [13] results (obtained w/o fit to E40 data). Although NLO19 reproduces the E40 data in Fig. 4a) and b), it failed to reproduce in Fig. 4c). However, a parameter of NLO19 can be easily readjusted to fit without influencing other results, as shown by dotted lines, NLO19(600). As in Table. 1, Fig. 4c) is $I=3/2$ and sensitive to 10-plet, which does not appear in NN interactions. More parameter separations are achieved by adding spin observables. J-PARC E86 experiment was proposed to measure the spin observables of Λp scatterings [14].

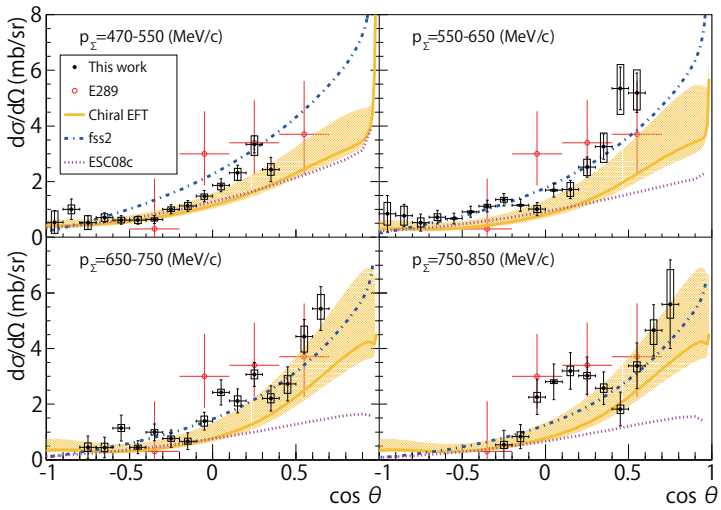

Figure 3: [E40] Differential cross section for $\Sigma^- p$ elastic scattering. Adopted from [9]

3.3 J-PARC E13 experiment - charge symmetry breaking of s-orbit hyper nucleus

Charge symmetry in nuclear physics, the similarity of the strong interactions of pp and nn is well established. The binding energies of ^{3}H and ^{3}He , a pair of mirror nuclei, only differ by 70 keV

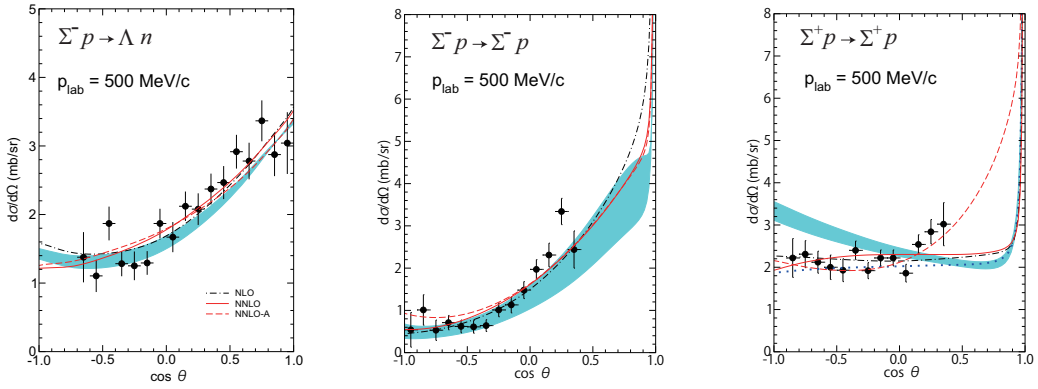

Figure 4: Cross sections obtained by EFT compared with E40 data. Cyan band is NLO19. Solid line is NNLO. Dotted line is NLO19(600) with a parameter readjusted. Adopted from [12] (CC4.0).

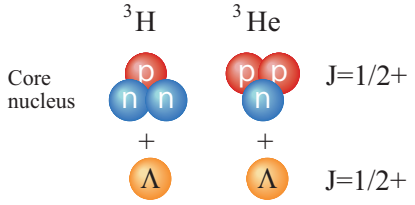

Figure 5: [E13] Cartoon of ${}^4_\Lambda$H and ${}^4_\Lambda$He. The system is a bound state of a core nucleus (either ^{3}H or ^{3}He) and Λ. The core nucleus and Λ have $J^P = 1/2^+$, forming 1^+ or 0^+ s states.

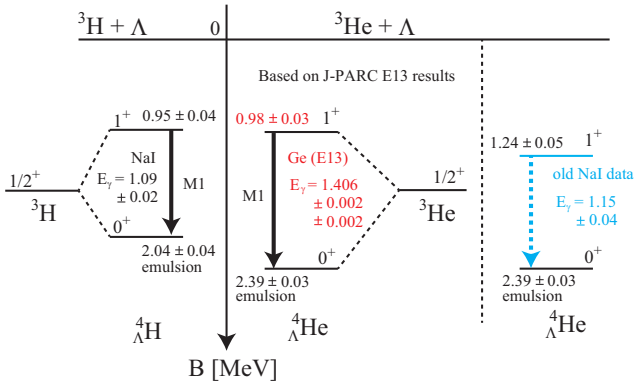

Figure 6: [E13] Level diagrams for the $A = 4$ hypernuclei. Modified based on [15]. J-PARC E13 measured M1 transition ${}^4_\Lambda\mathrm{He}(1^+) \to (0^+)$.

after Coulomb correction. It was assumed that the symmetry holds for ΛN interactions. Figure 5 illustrates the $A = 4$ Λ hypernuclei. ${}^4_\Lambda$H(${}^4_\Lambda$He) is a bound state of a core nucleus ^{3}H(^{3}He) and Λ, both having $J^P = 1/2^+$. The resulting system has 1^+ or 0^+ when Λ is in s-orbit.

Figure 6 depics level diagram of $A = 4$ Λ hypernuclei [15]. Old emulsion experiments measured the binding energy of the ground states for ${}^4_\Lambda\mathrm{H}(0^+)$ and ${}^4_\Lambda\mathrm{He}(0^+)$ and are 2.04 ± 0.04 MeV and 2.39 ± 0.03 MeV, respectively [16]. The values result in large charge symmetry breaking (CSB), $\Delta B_\Lambda(0^+) = B_\Lambda({}^4_\Lambda\mathrm{He}) - B_\Lambda({}^4_\Lambda\mathrm{H}) = 0.35 \pm 0.05$ MeV, where binding energy B_Λ is defined as $B_\Lambda = (M_{\mathrm{core}} + M_\Lambda) - M_{\mathrm{hypernuclei}}$. Theoretical considerations fail to give $\Delta B_\Lambda(0^+)$ of more than 100 keV. M1 transition measurements give energy difference between 1^+ and 0^+ states. Old measurements using NaI reported $E_\gamma = 1.09 \pm 0.02$ for ${}^4_\Lambda$H and $E_\gamma = 1.15 \pm 0.04$ MeV, suggesting large CSB even in $\Delta B_\Lambda(1^+) = 0.29 \pm 0.06$ MeV (See [15] for details). However, the latter measurement, blue text in Fig. 6, is statistically insufficient and ambiguous.

To clarify the situation, the J-PARC E13 experiment performed a γ-ray spectroscopy for ${}^4_\Lambda$He by using germanium (Ge) detectors with an order of magnitude better energy resolution than NaI. The 1^+ excited state of ${}^4_\Lambda$He was produced via ${}^4\mathrm{He}(K^-, \pi^-)$ reaction with a 1.5 GeV/c K^- beam.

The γ-rays were measured by Hyperball-J [17], Ge detector array surrounding the experimental target. The array consists of 27 Ge detects equipped with $PbWO_4$ counters surrounding each Ge crystal to suppress background events such as Compton scattering and high energy γ from π^0 decay.

Figure 7 depicts the missing mass distribution for ${}^{4}_{\Lambda}$He as a function of the excitation energy, $E_{\rm ex}$. As indicated in the figure, $-4 < E_{\rm ex} < +6$ MeV was selected to look for the γ-ray spectrum, which is shown in Fig. 8. The upper (lower) histogram is obtained without (with) event-by-event Doppler correction. E13 measured unambiguously the M1 transition, and was $1406 \pm 2(stat) \pm 2(syst)$ keV as the red text beside the M1 arrow in Fig. 6. This value is significantly different from the ${}^{4}_{\Lambda}$H spacing of 1.09 ± 0.02 MeV, confirming the existence of CSB in the ΛN interaction. Using emulsion data of $B_\Lambda(0^+)$, the E13 data indicates CSB is only prominent in 0^+, therefore, spin-dependent. It suggests $\Lambda - \Sigma$ mixing, whose effect is an order of magnitude smaller in 1^+, is responsible for CSB. J-PARC E63 [18] was proposed to improve the precision of the M1 transition for ${}^{4}_{\Lambda}$H with Ge detectors. An update of ground-state energies is also expected from the reanalysis of E07 emulsions.

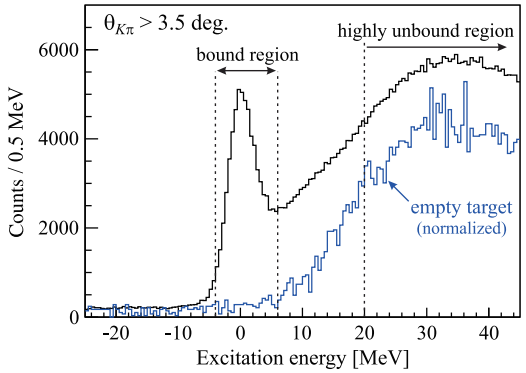

Figure 7: [E13] Missing mass distribution for ${}^{4}_{\Lambda}$He in the reaction ^{4}He$(K^-, \pi^-){}^{4}_{\Lambda}$He, plotted as a function of the excitation energy. The black (blue) histogram is obtained with (without) liquid helium in the target vessel. Adopted from [15].

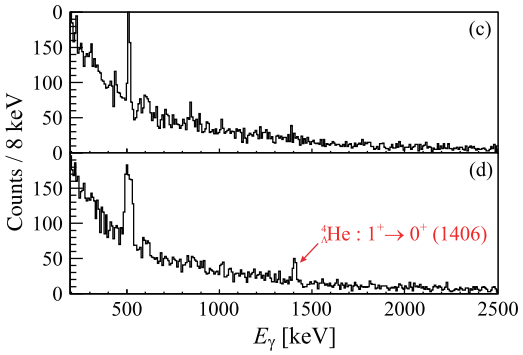

Figure 8: [E13] Obtaind γ energy spectrum after identifying ${}^{4}_{\Lambda}$He by selecting the bound region in missing mass. Upper and lower panels were obtained without and with event-by-event Doppler correction, respectively. Adopted from [15].

3.4 J-PARC E07 experiment: $S = -2$ system using nuclear emulsion

Compared to relatively well-explored $S = -1$ hypernucleus, experimental information of $S = -2$ is still very limited. KEK-E373 experiment successfully observed KISO event [19] using nuclear emulsion[1], which is unambiguously identified as $\Xi^- + {}^{14}N \rightarrow {}^{10}_{\Lambda}\mathrm{Be} + {}^{5}_{\Lambda}\mathrm{He}$. The binding energy of the Ξ^-, B_{Ξ^-} was deduced to be $B_{\Xi^-} = 3.87 \pm 0.21$ MeV or 1.03 ± 0.18 MeV, depending on whether the daughter ${}^{10}_{\Lambda}$Be was produced in the ground or excited state. J-PARC E07 investigated $S = -2$ systems further using a hybrid emulsion method. 1.81 GeV/c K^- irradiated a diamond target with a thickness of 9.87 g/cm^2. Ξ^- was produced via quasi-free $p(K^-, K^+)\Xi^-$ reactions, entering into a downstream emulsion. Outgoing K^+ was analyzed by KURAMA spectrometer, identifying Ξ^- production by missing mass. The predicted position and direction of Ξ^- by electronic counters were used to search for events in the emulsions, hence named hybrid. Figure 9 displays IBUKI

[1] Although KEK E373 adopted hybrid method, KISO event was found by a general scan, where events were searched without information from electronic counters.

event [20] measured by E07, which is the first uniquely identified Ξ hypernuclear state ($\Xi^-_{1p}-{}^{14}$N), decaying into two Λ hypernuclei. Binding energy was measured as $B_\Xi^{1p} = 1.27 \pm 0.21$ MeV. Figure 10 depicts the IRRAWADDY event [21]. It was claimed to be the first observation of the nuclear *s*-state of Ξ hypernucleus and assigned as $\Xi^- + {}^{14}\mathrm{N} \to {}^{5}_{\Lambda}\mathrm{He} + {}^{5}_{\Lambda}\mathrm{He} + {}^{4}\mathrm{He} + n$. The binding energy was determined to be $B_{\Xi^-} = 6.27 \pm 0.27$ MeV. However, E. Friedman and A. Gal discuss a different interpretation that the state is Ξ^0_{1p} – ^{14}C slightly admixed by Ξ^-_{1p} – ^{14}N [22]. $\Xi^0 + {}^{14}$C threshold is 6.18 MeV below the $\Xi^- + {}^{14}$N, making the actual binding energy smaller by that amount. Analysis of hypernuclei suggests a stronger Ξ*N* attraction than ΛΛ and a weak Ξ*N* – ΛΛ coupling, consistent with femtoscopic studies by ALICE [23] and HAL QCD calculations [24].

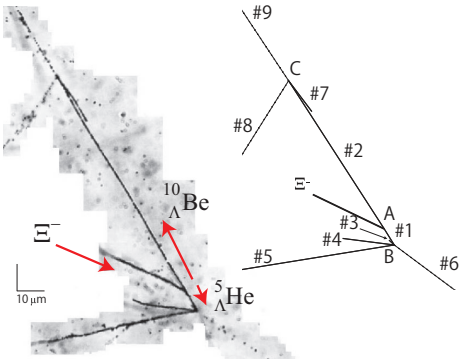

Figure 9: [E07] IBUKI event. $\Xi^- + {}^{14}\mathrm{N} \to {}^{10}_{\Lambda}\mathrm{Be}(\#1) + {}^{5}_{\Lambda}\mathrm{He}(\#2)$. Adopted from [20].

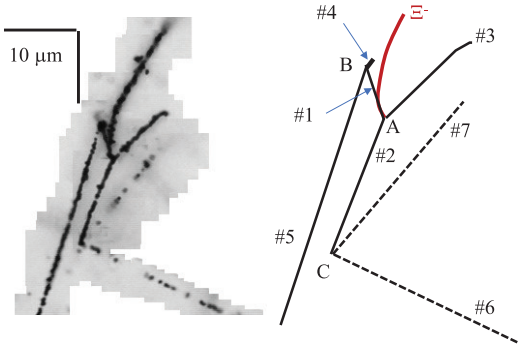

Figure 10: [E07] IRRAWADDY event. $\Xi^- + {}^{14}\mathrm{N} \to {}^{5}_{\Lambda}\mathrm{He}(\#1) + {}^{5}_{\Lambda}\mathrm{He}(\#2) + {}^{4}\mathrm{He}(\#3) + n$. Adopted from [21] (CC4.0).

3.5 J-PARC E05 and E70 experiment: $S = -2$ system using counters

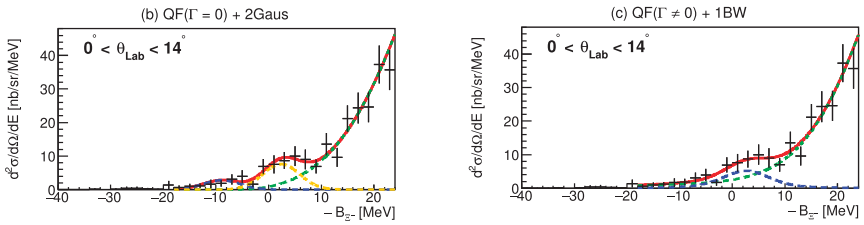

Figure 11: [E05] Missing mass distribution as a function of $-B_\Xi$. A negative value corresponds to the bound region. Two scenarios out of five yielded reasonable χ^2 and are shown. The Green lines represent QF. The Yellow and blue lines are two Gaussians. The blue line is BW. Adopted from [25] (CC4.0).

Based on results using nuclear emulsions, partly presented in Sec. 3.4, Ξ*N* interaction is considered to be attractive, but a small event sample is insufficient to obtain detailed information. J-PARC E05 measured missing mass of the ${}^{12}C(K^-, K^+)$ reactions at 1.8 GeV/*c*, where Ξ^- hypernucleus is directly produced [25]. K^- momentum is analyzed by the beam line spectrometer and out-going K^- was analyzed by the Superconducting Kaon Spectrometer (SKS) [26] configured in SksMinus setup [15]. The design momentum resolution of the beamline is $\Delta p/p = 3.3 \times 10^{-4}$ (FWHM). The momentum of outgoing K^+ is about 1.4 GeV/*c* and the achieved resolution at 1.35 GeV/*c* was

$\Delta p/p = 3.6\times10^{-3}$ (FWHM). A missing mass resolution of 8.2 MeV (FWHM) was obtained, better than the 14 MeV of the BNL-E885 experiment [27].

The differential cross section was obtained as a function of the binding energy of Ξ^-. The background subtracted spectrum was consistent with BNL E885 experiments. They analyzed the spectrum with five scenarios. Two of them yielded similar and reasonable χ^2 and are shown in Fig. 11. Figure 11 (left) was fitted with a quasi-free (QF) smooth component and two Gaussians. Figure 11 (right) was fitted with QF + Breit-Wigner (BW) component. BW was tried having $\Xi N \to \Lambda\Lambda$ conversion effect in mind, although theoretically, it is considered small. QF-only fit and QF + 1 Gaus fit showed worse χ^2. Limited resolution prevented the determination of the binding energy; however, it was clearly shown that there is a structure near the threshold. To determine the binding energy of Ξ-hypernuclear states, improvement in energy resolution is necessary.

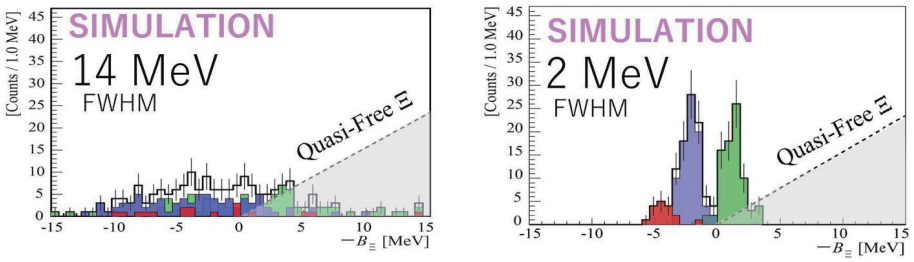

Figure 12: [E70] Simulated missing mass distributions with 14 MeV (left) and 2 MeV (right) resolution under the same theoretical prediction. Adopted from [28] (CC4.0).

J-PARC E70 is a successor of E05 and is being conducted. The spectrometer was upgraded to use the S-2S spectrometer, improving the momentum resolution to $\Delta p/p = 6\times10^{-4}$ (FWMH) [28]. An Active Fiber Target (AFT), which is composed of scintillation fibers is used to measure the energy straggling of charged particles in the target. A missing mass resolution of 2 MeV (FWMH) is expected to be achieved with the event-by-event energy-loss correction. It is seven times compared to the BNL-E885 experiment and four times better compared to J-PARC E05. Figure 12 displays an expected missing mass spectra with the design resolution, demonstrating discrimination capability.

4. K1.8BR beamline

4.1 J-PARC E15 experiment - $\bar{K}NN$ system

$\bar{K}N$ interaction is strongly attractive in the iso-singlet ($I = 0$) channel as studied by kaonic hydrogen atoms and a $\bar{K}N$ scattering experiment. The $\Lambda(1405)$ was proposed to be a $\bar{K}N$ molecule state [29], and the interpretation is now widely accepted [30, 31]. The natural extension of the system is larger kaoninc nuclei with more nucleons, such as $\bar{K}NN$, and $\bar{K}NNN$. J-PARC E15 conducted exclusive measurement of $K^-+{}^3\mathrm{He} \to \Lambda pn$ reactions to search for $\bar{K}NN$ state [32]. 1 GeV/c of K^- beam irradiated a liquid ^{3}He target. $\Lambda(\to \pi^- p)$ and p are detected by a cylindrical detector system (CDS) consisting of a cylindrical drift chamber and a scintillator hodoscope installed in a solenoid magnet. The outgoing n was identified by the missing mass.

Their observation is consistent with a two-step process as illustrated in Fig. 13. An elementary reaction occurs between incident K^- and one of the nucleons in the ^{3}He target, $K^-+N \to \bar{K}+n$. The

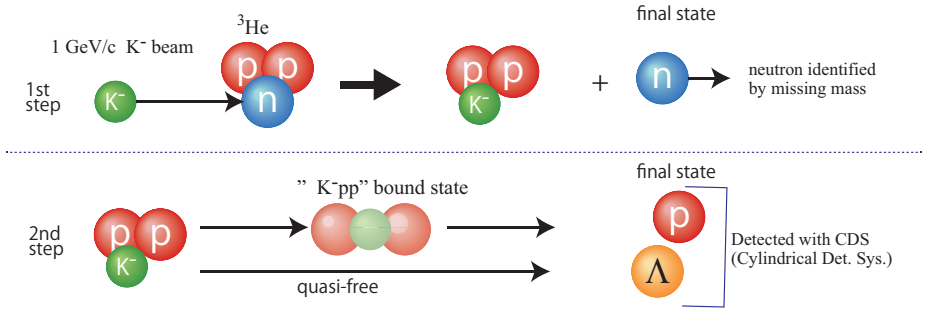

Figure 13: [E15] Illustration of a two-step production process. Incident K^- collides and knocks out a neutron. ($K^- + n \to K^- n$.) The recoil K^- is off-shell to form $K^- pp$ bound state with the spectator pp, decaying into Λp. When the recoil K^- is on-shell it still can be absorbed by the spectator pp to result in the Λp final state (quasi-free). The 1st step could be $K^- p \to \bar{K}^0 n$, resulting in $\bar{K}^0 np$ bound state or quasi-free reaction with the same final state Λp and knocked-out n.

beam momentum of 1 GeV/c was chosen to maximize this elementary reaction to occur. Off-shell $\bar{K}$ may form a bound state $\bar{K}NN$, with two spectator nucleons and decay into YN (Λp). On-shell $\bar{K}$ may also be absorbed by two spectator nucleons, resulting in YN final state (quasi-free process). Both can be denoted as $\bar{K}NN \to YN$ (Λp in E15).

Momentum transfer q_X is defined as $q_X = |\mathbf{p}^{\rm lab}_{\mathbf{K}^-} - \mathbf{p}^{\rm lab}_{\mathbf{n}}|$, where $\mathbf{p}^{\rm lab}_{\mathbf{K}^-}$ and $\mathbf{p}^{\rm lab}_{\mathbf{K}^-}$ are momenta of incident K^- and outgoing n in the lab frame, respectively. The two-step interpretation suggests that q_X is the $\bar{K}$ momentum and is the momentum of YN, but the Fermi motion smears the actual momentum. Figure 14 shows q_X vs the invariant mass of Λp, m_X after acceptance correction. There exists a momentum transfer independent component below $\bar{K}NN$ mass and above Λp mass, which was identified as $\bar{K}NN$ bound state. The blue dotted line describes the expectation from the quasi-free process whose centroid is,

$$M_F(q_X) = \sqrt{4m_N^2 + m_{\bar{K}}^2 + 4m_N\sqrt{m_{\bar{K}}^2 + q_X^2}}. \tag{1}$$

and such component is also visible in the plot. Two loci exist on the quasi-free expectation line; one corresponds to $\theta_n = 0$, and the other corresponds to $\theta_n = \pi$. The 2D spectrum was well-fitted as in Fig. 15 with their model, which includes $\bar{K}NN$ bound state, quasi-free process, and a "broad" distribution where energies are distributed according to the phase space. $\bar{K}NN \to \Sigma^0 p \to \Lambda\gamma p$ also contribute. The formula for the component that describes the bound state is,

$$\sigma(M,q) \propto \rho(M,q) \times \frac{\Gamma_{Kpp}/2}{(M - M_{Kpp})^2 + (\Gamma_{Kpp}/2)^2} \times \exp\left(-\frac{q^2}{Q_{Kpp}^2}\right), \tag{2}$$

where $\rho(M,q)$ is the phase space, the second term is Breit-Wigner distribution with a mass M_{Kpp} and a width Γ_{Kpp}, the last term is a Gaussian form factor. The mass was determined as $M_{Kpp} = 2.328 \pm 0.003(\text{stat})^{+0.004}_{-0.003}(\text{syst})$ GeV/c^2 thus have a large binding energy of 40 MeV/c^2. The Breit-Wigner width was $\Gamma_{Kpp} = 100 \pm 7(\text{stat})^{+19}_{-9}(\text{syst})$, twice as large as $\Lambda(1405)$, and S-wave gaussian form factor was obtained to be $Q_{Kpp} = 383 \pm 11(\text{stat})^{+4}_{-1}(\text{syst})$ MeV/c. Such a large Q_{Kpp} may indicate that the produced state is a compact system as $R = \frac{\hbar}{Q}\frac{2m_N + m_{\bar{K}}}{2m_N} \sim 0.6$ fm.

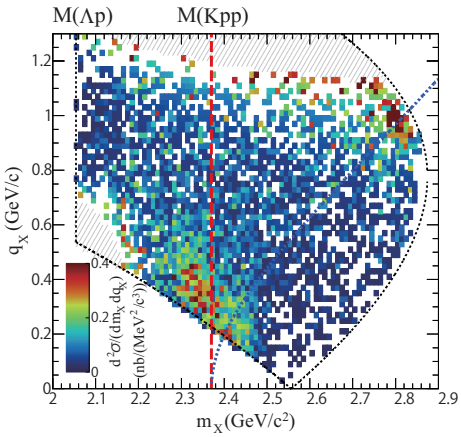

Figure 14: [E15] Momentum transfer q_X vs invariant mass m_X after acceptance correction. The black dotted outer lines indicate the kinematical limit of the reaction. The vertical red dotted line is the mass of $\bar{K}NN$, $m_{\bar{K}+2m_N} \sim 2.37$ GeV/c^2. The blue dotted line describes the expectation from the quasi-free process. See text for details. Modified based on [32]

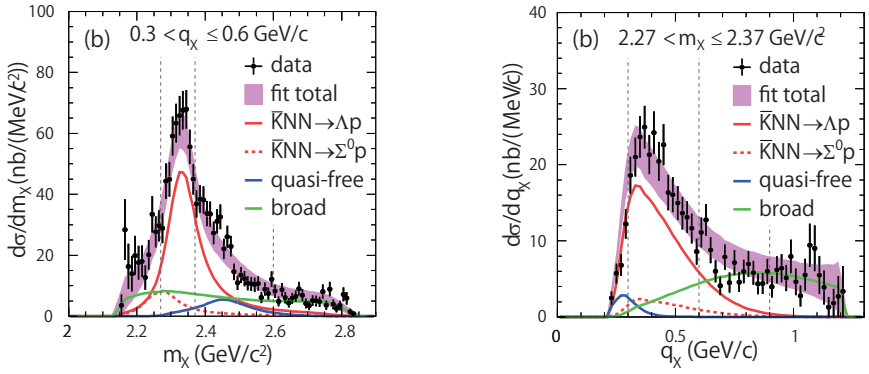

Figure 15: [E15] Left) Invariant mass (m_X) distribution for the momentum range of 0.3–0.6 GeV/c. Right) Momentum transfer (q_X) distribution for invariant mass (m_X) interval of 2.27–2.37 GeV/c^2. Their model-fitting results are overlaid. Adopted from [32]

E15 measured mesonic decay channels of $\bar{K}NN \to \pi YN$ [33] since the branching ratio gives information of the size of the system. Although statistics were limited, preliminary $\bar{K}NNN$ results were also obtained. J-PARC E80 was proposed to continue the effort, upgrading detector to achieve 1.6 times larger solid angle, 4 times higher neutron detection efficiency. They aim to start taking data in JFY2026. The experiment is to confirm the existence of the $\bar{K}NNN$ state, to study in detail $\bar{K}NN$ states by determining spin-parity and searching for isospin partner K^-pn (J-PARC E89).

5. High-p beamline

5.1 J-PARC E16 experiment - ϕ meson in nucleus

J-PARC E16 experiment is to measure in-medium spectral change of vector mesons via e^+e^- decay at 30 GeV p+A (C, Cu, later CH2 and Pb) collisions [34] as a signal of partial restoration of spontaneously broken chiral symmetry. KEK-E325 experiment measured the same reaction in p+C

and Cu at 12 GeV. Their observation suggests that ϕ meson mass reduces by $3.4^{+0.6}_{-0.7}$% and the width increases by $3.6^{+1.8}_{-1.2}$ times at nuclear saturation density [35]. E16 aims to collect six times more statistics in the first phase, Run 1, with an improved ϕ mass resolution of 5.8 MeV/c^2 for $\beta\gamma < 0.5$, compared to the measured resolution of 10.7 MeV/c^2 for E325.

Figure 16 depicts expected ϕ mass spectra for $\beta\gamma < 1.25$ based on E325 interpretation. The red line is an expectation from the vacuum shape under experimental effects. Clear excess in the lower side of the mass can be identified. Reasonable χ^2 can be obtained only by excluding the excess region indicated by the vertical green lines. Figure 17 shows excess fractions vs $\beta\gamma$. Green points are expected in Run 1 while pink points are from E325 where only the lowest $\beta\gamma$ is significant. The tendency becomes clearer and more significant compared to E325 results. E16 is also going to measure the momentum dependence of the mass — namely the dispersion relation — for hadrons for the first time.

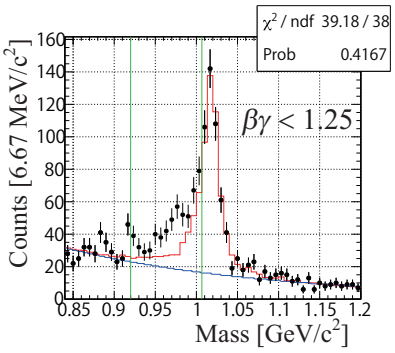

Figure 16: [E16] ϕ mass spectrum expected in Run 1.

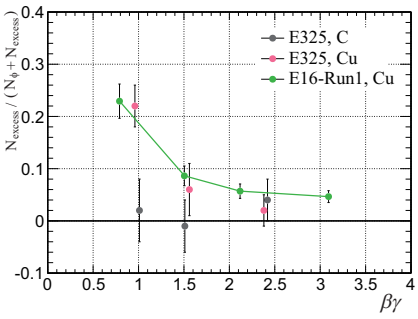

Figure 17: [E16] $\beta\gamma$ dependence of excess fraction expected in Run 1.

All detectors were already prepared for Run 1. Particle tracking is performed by a layer of Silicon Tracking System (STS), and three layers of Gas Electron Multiplier Trackers (GTR). Electron identification (EID) is performed by Hadron Blind Chrenkov Detectors (HBD) and leadglass calorimeters (LG). All are installed in a dipole magnet. Figure 18 displays a clear correlation between energy loss and momentum of corresponding particle species, demonstrating a successful operation of STS which was developed with GSI-CBM and newly installed in 2023. E16 uses LG as EID, and thickness (8 X_0) is insufficient for precise total energy measurement. Nevertheless, as shown in Fig. 19, LG exhibits a clear E/p correlation under electron enhancement by HBD, demonstrating excellent EID capability under a high counting environment.

6. Future projects

6.1 HEF-ex: Hadron Experimental Facility Extention project

The Hadron Experimental Facility Extention project, HEF-ex [36], was proposed to extend the Hadron hall, adding more beamlines with additional functionalities [37]. The project was selected as the top priority at the KEK Project Implementation Plan (PIP) 2022. KEK requests budgets for MEXT based on PIP. $g-2$ was elected in previous PIP and HEF-ex is in line after $g-2$. Figure 20 illustrates a plan of the extended hadron hall with new beamlines.

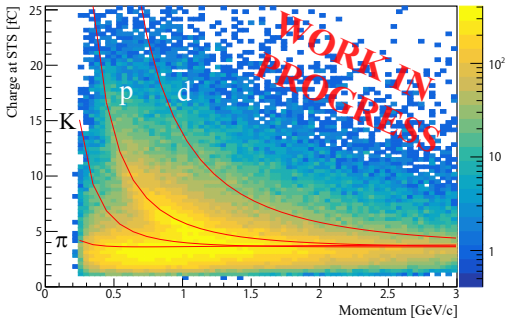

Figure 18: [E16] Energy loss at STS vs momentum.

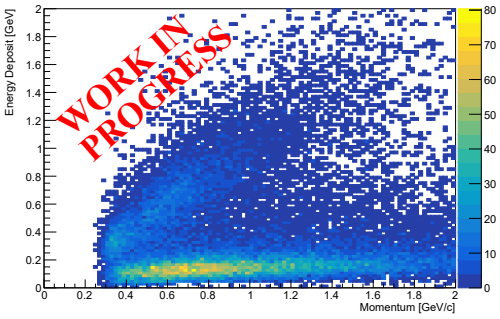

Figure 19: [E16] E-p relation by LG, under electron enhancement by HBD.

High Intensity High Resolution (HIHR) beamline provides mass-separated secondary beams of up to 2 GeV/c using the dispersion matching technique [38]. J-PARC P84 will perform a systematic Λ hypernuclear spectroscopy up to a Pb target with an unprecedented missing-mass resolution of 0.4 MeV/c^2, which reveals three-body forces to solve the hyperon puzzle. K10 beamline provides mass-separated secondary beams of up to 10 GeV/c, making Ω (P89 [39]) and Ξ^* spectroscopy possible. A polarized Λp scattering experiment will be performed at K1.1 [14]. KOTO-II measures CP violating decay $K_L \to \pi^0 \nu\bar{\nu}$ with more than 5 σ under the SM prediction at thew new KL beamline [40].

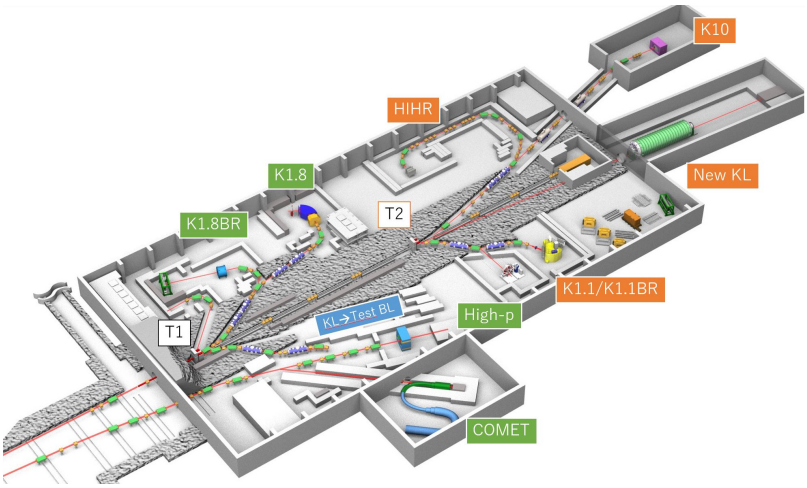

Figure 20: Illustration of the extended experimental facility with proposed new beamlines, HIHR, K1.1/K1.1BR, K10 and new KL.

6.2 J-PARC HI: Heavy ion project

J-PARC plans to accelerate heavy ions. With the available energy range of 1–12A GeV for Au beam, highly dense matter with 5–10 times the saturation density can be created. QCD phase structure can be explored, such as QCD critical point, first-order phase transition, and precursor phenomena of color superconductivity. J-PARC takes a step-by-step approach, and the final goal

of the beam intensity is 10^{11} Hz. J-PARC P87 was proposed as the first step to start with upgraded J-PARC E16 detectors, adding a new ion injector and existing booster synchrotron [41].

7. Summary

J-PARC is a multi-purpose accelerator complex that enables materials and life sciences and nuclear and particle physics research. Some experimental results and ongoing experiments at HD were reviewed, including hyperon scattering experiments, hypernuclear spectroscopy, and the study of mesons in exotic states. Future projects such as the Hadron experimental facility hall extension (HEF-ex) and heavy ion project (J-PARC HI) aim to expand these studies. These efforts continue to give insights into and reveal the nature of strongly interacting systems at multiple scales.

References

[1] T. Mibe [J-PARC g-2], Nucl. Phys. B Proc. Suppl. **218**, 242-246 (2011)

[2] M. Harada *et al.* [JSNS2], arXiv:1310.1437 [physics.ins-det]

[3] Y. Fuwa *et al.*, arXiv:2412.19519 [nucl-ex]

[4] J-PARC 38th PAC approval summary for particle and nuclear experiments, https://j-parc.jp/researcher/Hadron/en/pac_2407/J-PARC-PAC-38-final_240930.pdf

[5] J.K. Ahn *et al.*, arXiv:2411.11237 [hep-ex]

[6] E. Hirose *et al.*, IEEE Trans. Appl. Supercond. **32**, no.6, 4101904 (2022)

[7] K. Shirotori *et al.*, [J-PARC E50] this volume.

[8] Y. Akazawa *et al.* [J-PARC E40] Nucl. Instrum. Meth. in Phys. Res. A **1029**, 166430 (2022)

[9] K. Miwa *et al.* [J-PARC E40] Phys. Rev. C **104**, 045204 (2021)

[10] T. Nanamura *et al.* [J-PARC E40] Prog. Theor. Exp. Phys. **2022**, 093D01 (2022)

[11] K. Miwa *et al.* [J-PARC E40] Phys. Rev. Lett. **128**, no.7, 072501 (2022)

[12] J. Haidenbauer, U. G. Meißner, A. Nogga and H. Le, Eur. Phys. J. A **59**, 63 (2023)

[13] J. Haidenbauer, *et al.*, Eur. Phys. J. A **56**, 91 (2020)

[14] [J-PARC P86] Differential cross section and spin observables of the Λp scattering https://j-parc.jp/researcher/Hadron/en/pac_2107/pdf/P86_2021-14.pdf

[15] T. O. Yamamoto *et al.* [J-PARC E13], Phys. Rev. Lett. **115**, 222501 (2015)

[16] M. Juric *et al.*, Nucl. Phys. B **52**, 1 (1973)

[17] T. Koike *et al.*, Proceedings of the 9th International Conference on Hypernuclear and Strange Particle Physics (HYP2006), Mainz, Germany, 2006

[18] H. Tamura, this volume.

[19] K. Nakazawa *et al.* [KEK-E373] Prog. Theor. Exp. Phys. **2015**, 033D02 (2015)

[20] S. H. Hayakawa *et al.* [J-PARC E07] Phys. Rev. Lett. **126**, 062501 (2021)

[21] M. Yoshimoto *et al.* [J-PARC E07/KEK-E373] Prog. Theor. Exp. Phys. **2021**, 073D02 (2021)

[22] E. Friedman and A. Gal., Phys. Lett. B **837**, 137640 (2023)

[23] S. Acharya *et al.*, Phys. Rev. Lett. **123**, 112002 (2019)

[24] K. Sasaki *et al.*, Nucl. Phys. A **998**, 121737 (2020)

[25] Y. Ichikawa *et al.*, Prog. Theor. Exp. Phys. **2024**, 091D01 (2024)

[26] T. Takahashi *et al.*, Prog. Theor. Exp. Phys. **2012**, 02B010 (2012)

[27] P. Khaustov *et al.*, Phys. Rev. C **61**, 054603 (2000)

[28] T. Gogami *et al.*, EPJ Web of conferences **271**, 11002 (2022)

[29] E. A. Veit *et al.*, Phys. Rev. D **31**, 1033 (1985)

[30] J. M. M. Hall *et al.*, Phys. Rev. Lett. **114**, 132002 (2015)

[31] T. Waas, N. Kaiser and W. Weise, Phys. Lett. B **379**, 34-38 (1996)

[32] T. Yamaga *et al.*, [J-PARC E15] Phys. Rev. C **102**, 044002 (2020)

[33] T. Yamaga *et al.*, [J-PARC E15] Phys. Rev. C **110**, 014002 (2024)

[34] K. Aoki *et al.*, [J-PARC E16] J. Subatomic Part. Cosmol. **3**, 100019 (2025)

[35] R. Muto *et al.* [KEK-PS-E325] Phys. Rev. Lett. **98**, 042501 (2007)

[36] https://www.rcnp.osaka-u.ac.jp/~jparchua/en/hefextension.html

[37] K. Aoki *et al.*, arXiv:2110.04462 [nucl-ex].

[38] [J-PARC P84] High precision spectroscopy of Λ hypernuclei at HIHR.
https://j-parc.jp/researcher/Hadron/en/pac_2107/pdf/P84_2021-08.pdf

[39] [J-PARC P85] Spectroscopy of Omega baryons
https://j-parc.jp/researcher/Hadron/en/pac_2107/pdf/P85_2021-10.pdf

[40] [J-PARC P107] Proposal of the KOTO II experiment, arXiv:2501.14827 [hep-ex].

[41] [J-PARC P87] Dielectron measurements in heavy-ion collisions at J-PARC with E16 upgrades.
https://j-parc.jp/researcher/Hadron/en/pac_2107/pdf/P87_2021-13.pdf